Title

Lipid-enriched diet rescues lethality and slows down progression in a murine model of VCP-associated disease.

Journal

Human Molecular Genetics, 23(5)

Authors

Llewellyn, Katrina
Nalbandian, Angèle
Jung, Kwang-Mook
et al.

Publication Date

2014-03-01

DOI

10.1093/hmg/ddt523

Peer reviewed

Human Molecular Genetics, 2014, Vol. 23, No. 5 **1333–1344**
doi:10.1093/hmg/ddt523
Advance Access published on October 24, 2013

Lipid-enriched diet rescues lethality and slows down progression in a murine model of VCP-associated disease

Katrina J. Llewellyn[1,†], Angèle Nalbandian[1,†,*], Kwang-Mook Jung[2], Christopher Nguyen[1], Agnesa Avanesian[2], Tahseen Mozaffar[3], Daniele Piomelli[2,4] and Virginia E. Kimonis[1,*]

[1]Department of Pediatrics, Division of Genetics and Metabolism, [2]Department of Anatomy and Neurobiology and [3]Department of Neurology, Orthopedic Surgery, University of California-Irvine, Irvine, CA 92697, USA and [4]Drug Discovery and Development, Istituto Italiano di Tecnologia, Genoa 16133, Italy

Received March 21, 2013; Revised August 30, 2013; Accepted October 17, 2013

Valosin-containing protein (VCP)-associated disease caused by mutations in the *VCP* gene includes combinations of a phenotypically heterogeneous group of disorders such as hereditary inclusion body myopathy, Paget's disease of bone, frontotemporal dementia and amyotrophic lateral sclerosis. Currently, there are no effective treatments for VCP myopathy or dementia. VCP mouse models carrying the common R155H mutation include several of the features typical of the human disease. In our previous investigation, $VCP^{R155H/R155H}$ homozygous mice exhibited progressive weakness and accelerated pathology prior to their early demise. Herein, we report that feeding pregnant $VCP^{R155H/+}$ heterozygous dams with a lipid-enriched diet (LED) results in the reversal of the lethal phenotype in $VCP^{R155H/R155H}$ homozygous offspring. We examined the effects of this diet on homozygous and wild-type mice from birth until 9 months of age. The LED regimen improved survival, motor activity, muscle pathology and the autophagy cascade. A targeted lipidomic analysis of skeletal muscle and liver revealed elevations in tissue levels of non-esterified palmitic acid and ceramide (d18:1/16:0), two lipotoxic substances, in the homozygous mice. The ability to reverse lethality, increase survival, and ameliorate myopathy and lipids deficits in the $VCP^{R155H/R155H}$ homozygous animals suggests that lipid supplementation may be a promising therapeutic strategy for patients with VCP-associated neurodegenerative diseases.

INTRODUCTION

Hereditary inclusion body myopathy, Paget's disease of bone, and frontotemporal dementia (IBMPFD) caused by mutations in the *VCP* gene is associated with weakness and atrophy of skeletal, pelvic and shoulder girdle muscles in 90% of individuals (1–4). Affected individuals exhibit scapular winging, progressive muscle weakness and die from cardiac and respiratory failure (1,5). Histologically, patients display rimmed vacuoles and TAR DNA-Binding Protein-43 (TDP-43)-positive, ubiquitinated inclusion bodies in muscles (1,5–7). Variable phenotypes include limb girdle muscular dystrophy (LGMD) or amyotrophic lateral sclerosis (ALS).

VCP disease is increasingly being recognized, with >31 *VCP* mutations having been identified worldwide. The R155H mutation is by far the most common, accounting for~50% of affected individuals. VCP, a member of the type II AAA+ ATPase family, plays important roles in a plethora of cellular activities. Mutations in *VCP* are primarily within the N-terminal domain, which is involved in ubiquitin binding and protein–protein interactions. Our recent microarray studies in muscle indicate that multiple signaling pathways are dysregulated in patients with VCP-associated inclusion body myopathy, which include abnormalities in the actin cytoskeleton, ErbB signaling, cancer, regulation of autophagy and lysosomal signaling transduction cascades (8). Previous studies in patient myoblasts have implicated autophagy in the pathogenesis of VCP-associated disease (9,10).

Autophagy occurs through a multi-step mechanism regulated by autophagy-related proteins and is responsible for degrading

*To whom correspondence should be addressed at: Department of Pediatrics, Division of Genetics and Metabolism, University of California-Irvine, 2501 Hewitt Hall, Irvine, CA 92697, USA. Tel: +714 4565791; Fax: +714 4565330; Email: vkimonis@uci.edu
†The authors wish it to be known that, in their opinion, the first two authors should be regarded as joint First Authors.

and recycling defective organelles and maintaining cellular homeostasis. Inhibition of this process plays a critical role in the pathogenesis of several inherited myopathies (11). VCP is important in mediating protein degradation, a highly significant process for terminally differentiated cells. This protein is involved in the retro-translocation of misfolded endoplasmic reticulum (ER) proteins, and failure in its activity results in defective endoplasmic reticulum-associated degradation and ER stress responses. Autophagic degradation is thought to contribute to Alzheimer's and Huntington's diseases, among other neurodegenerative diseases, as well as in inflammatory disorders. Impaired autophagic degradation contributes to the pathogenesis of other human myopathies such as Danon disease (12), Pompe disease (13), sporadic inclusion body myositis (sIBM) (14) and Paget's disease of bone (PDB) (15). Mutations in the *Sequestosome 1* (*SQSTM1)* gene, which targets ubiquitinated protein aggregates for lysosomal degradation, have been associated with 10% of sporadic PDB, 50% of familial PDB cases and recently with ALS (16–21). Mitophagy, selective autophagy of mitochondria, is an important control mechanism that mediates the removal of damaged mitochondria in cells, whereby defects in this process have been implicated in neurodegeneration. VCP plays a critical role in maintaining mitochondrial quality and dynamics in the PINK1/Parkin pathway, whereby pathogenic mutations in *VCP* lead to an impairment in proteasome-dependent degradation (22) and induce mitochondrial uncoupling and reduced ATP levels in human neuroblastoma cells (23).

We have generated a novel neomycin cassette-free knock-in mouse model with the common disease-related R155H *VCP* mutation ($VCP^{R155H/+}$), which has features of human VCP-associated myopathy including progressive muscle, bone, spinal cord and brain pathology (24). The $VCP^{R155H/+}$ heterozygous mice demonstrate similar pathological characteristics observed in patients, however, have a slow rate of progression (24,25). Therefore, we developed the R155H homozygous ($VCP^{R155H/R155H}$) mouse model to investigate VCP disease pathogenesis and monitor responses to therapeutic strategies. $VCP^{R155H/R155H}$ homozygote mice exhibit progressive weakness prior to their early demise as well as accelerated pathology in skeletal muscle, spinal cord, brain and heart (26).

In the present study, we investigated the effects of a lipid-enriched diet (LED) on the $VCP^{R155H/R155H}$ homozygote mice. These mice appeared healthy, active and lived for several months rather than the maximum 21-day survival observed in mice fed a normal chow diet. The results suggest that LED administration may offer a novel treatment platform to slow down the progression of VCP-associated myopathies.

RESULTS

LED rescues homozygous $VCP^{R155H/R155H}$ animals

Placing pregnant $VCP^{R155H/+}$ heterozygote dams on a LED to increase their litter size led to the serendipitous finding of the homozygote rescue and survival. We monitored the weights and survival of the $VCP^{R155H/R155H}$ homozygous and wild-type (WT) mice on a LED (2019× Teklad Global Rodent Diet) versus their littermates on a normal diet (ND) (2020× Teklad Global Rodent Diet). $VCP^{R155H/R155H}$ mice fed a ND weighed an average of 6.97 g by 15 and 6.92 g by 21 days of age. The WT mice on a ND weighed an average of 8.63 g at 15 days, 11.35 g at 21 days, 18.85 g at 1 month, 23.10 g at 2 months, 28.40 g at 3 months, 27.95 g at 4 months and 34.55 g at 9 months of age, respectively. Blood ketone and glucose levels were assessed in these mice and did not show any significant differences between groups. $VCP^{R155H/R155H}$ animals on a LED depicted decreased adiposity, averaging 7.24 g by 15 days, 7.90 g by 21 days, 12.44 g by 1 month, 19.97 g by 2 months, 21.20 g by 3 months, 21.68 g by 4 months and 25.41 g by 9 months of age, respectively (Fig. 1A). In comparison, the WT animals on a LED revealed an accumulation of encapsulated adipose tissue, averaging 10.28 g by 15 days, 13.68 g by 21 days, 19.62 g by 1 month, 25.72 g by 2 months, 31.73 g by 3 months, 34.20 g by 4 months and 46.58 g by 9 months of age, respectively. Grip strength measurements were performed in the $VCP^{R155H/R155H}$ and WT animals on a LED and demonstrated significant improvement in muscle strengths (Fig. 1B). $VCP^{R155H/R155H}$ homozygous mice on a ND did not survive until weaning and were too weak for strength measurements ($P < 0.05$). The Kaplan–Meier survival rate among homozygous $VCP^{R155H/R155H}$ animals improved drastically on the LED versus their littermates on the ND ($P \leq 0.001$) (Fig. 1C); however, the diet did not completely reverse the lethality. There was no considerable difference in survival between WT animals on the ND and the LED.

To assess the short-term and long-term effects of LED, we performed histological analysis of quadriceps muscle in homozygous $VCP^{R155H/R155H}$ and WT littermates. Homozygous $VCP^{R155H/R155H}$ mice on the ND showed centrally localized nuclei, increased endomysial space between the muscle fibers and abnormal mitochondrial pathology as shown previously (26). In contrast, Hematoxylin and Eosin (H&E) staining of quadriceps muscles from $VCP^{R155H/R155H}$ animals on a LED at 3 weeks of age showed a significant improvement in muscle architecture (Fig. 1E) when compared with homozygotes on a ND (Fig. 1D). The 4-month- and 9-month-old $VCP^{R155H/R155H}$ animals, however, displayed progressive pathology of muscle quadriceps fibers on the LED including centrally localized nuclei and increased endomysial space between the fibers (Fig. 1F and G). This pathology was comparable with that seen in the heterozygote $VCP^{R155H/+}$ at 15 months (24), suggesting that homozygote $VCP^{R155H/R155H}$ mice fed a LED regimen may prove to be a useful tool for developing therapeutic strategies for VCP disease.

Electrodiagnostic studies reveal muscle improvement in the $VCP^{R155H/R155H}$ mice

Previously, we reported electromyography (EMG) evidence of acute and chronic denervation in the heterozygote $VCP^{R155H/+}$ mice (24.98 months ± 0.41) (25). These changes included abnormal spontaneous activity in the form of both fibrillation and fasciculation potentials and reduction in recruitment and interference patterns. Homozygous $VCP^{R155H/R155H}$ animals fed a ND showed motor unit abnormalities with reduced recruitment and interference (all traces are done at sensitivity of 100 microvolts and sweep of 10 ms). In contrast, the homozygous $VCP^{R155H/R155H}$ animals fed a LED showed motor units that approximated to those seen in the WT animals at 3 weeks of age (Fig. 2). WT ND and WT LED animals presented normal motor unit activation in response to noxious stimuli applied at the paws (Fig. 2A and B).

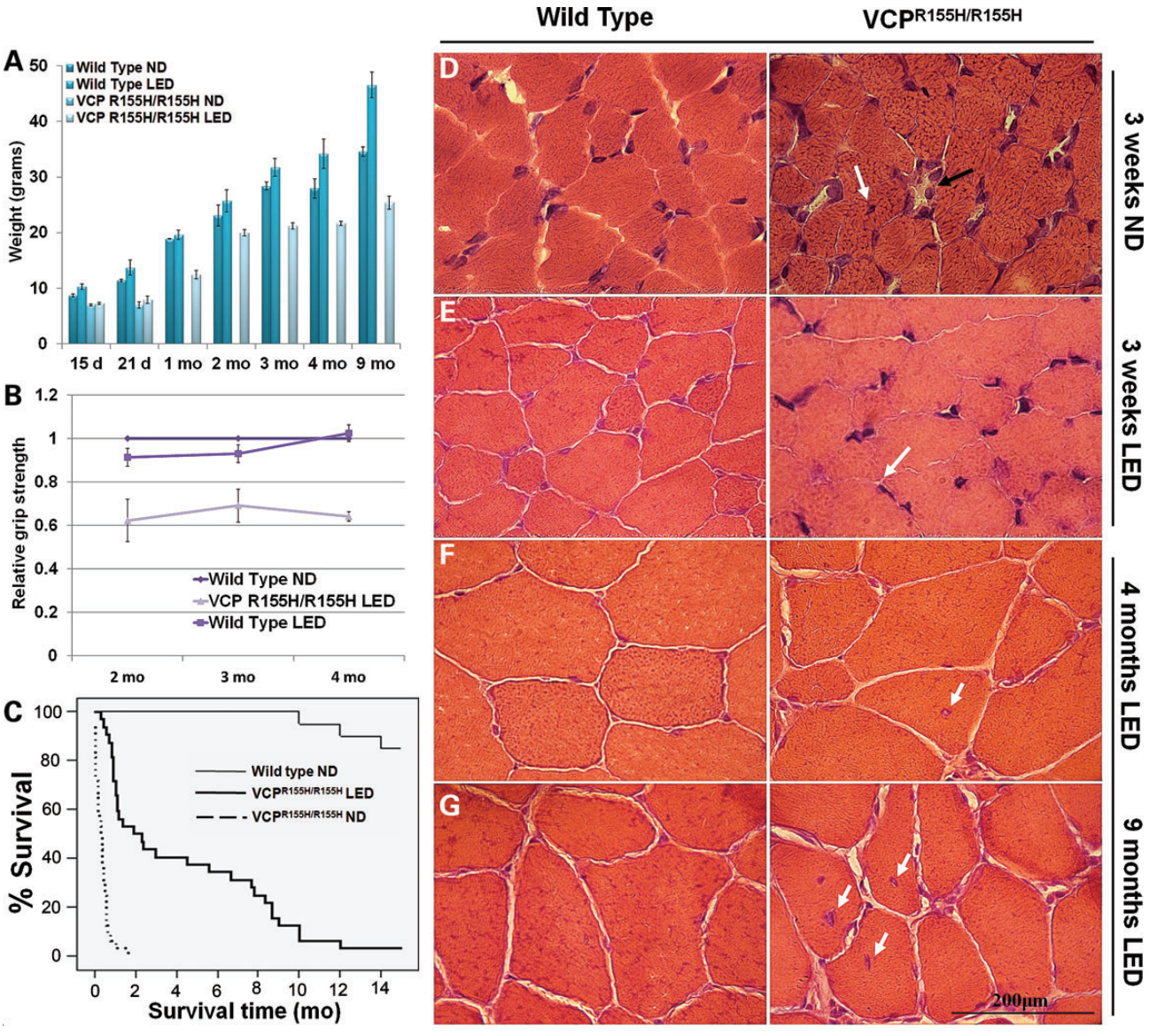

Figure 1. Measurements, survival curves and histological analyses of WT and $VCP^{R155H/R155H}$ mice on normal and LEDs. (**A**) Weight measurements, (**B**) grip strength analysis and (**C**) Kaplan–Meier survival curve of WT and $VCP^{R155H/R155H}$ mice ($P \leq 0.001$). H&E staining of quadriceps muscle from WT and $VCP^{R155H/R155H}$ animals at (**D** and **E**) 3 weeks of age depicting centrally located nuclei and necrosis (black arrows) on a ND and significant improvement in muscle architecture (arrows) on LED and (**F** and **G**) 4 months and 9 months of age showing centrally localized nuclei and increased endomysial space (black arrow), respectively, on normal versus LEDs (magnification: 630×). The number of mice analyzed per experiment is 5–6.

$VCP^{R155H/R155H}$ animals on a ND showed marked spontaneous activity (fibrillations) and sparse motor units of mixed morphology, suggestive of severe drop out of units (Fig. 2C). $VCP^{R155H/R155H}$ animals on a LED showed marked recovery of these units (Fig. 2D); the size of the units qualitatively was smaller than the WT, suggesting possible myopathic changes, but represented marked improvement over the ND-fed homozygote animals (Fig. 2D). These data are summarized in Fig. 2E.

Autophagy is stimulated in $VCP^{R155H/R155H}$ mice on LED

We have previously identified a dysfunction in the autophagic signaling cascade through accumulation of autophagy intermediates, such as protein p62/*SQSTM1* and Light Chain LC3-I/II, in $VCP^{R155H/R155H}$ animals versus their WT littermates (17). Autophagy was monitored by detection of endogenous LC3-I/II modification, ubiquitin-positive and p62-positive inclusions in the quadriceps of these mice. In comparison with the $VCP^{R155H/R155H}$ mice at 3 weeks of age on the ND (Fig. 3A, C, E, respectively), the LED-fed $VCP^{R155H/R155H}$ mice displayed an overall decrease in ubiquitinated proteins (Fig. 3B), a decrease in LC3-I expression followed by an increased conversion to LC3-II (Fig. 3D) and a decrease in p62 expression levels (Fig. 3F), suggesting an improvement of the autophagic process. Furthermore, we examined the TDP-43 aggregates (nuclear to cytoplasmic translocation) in

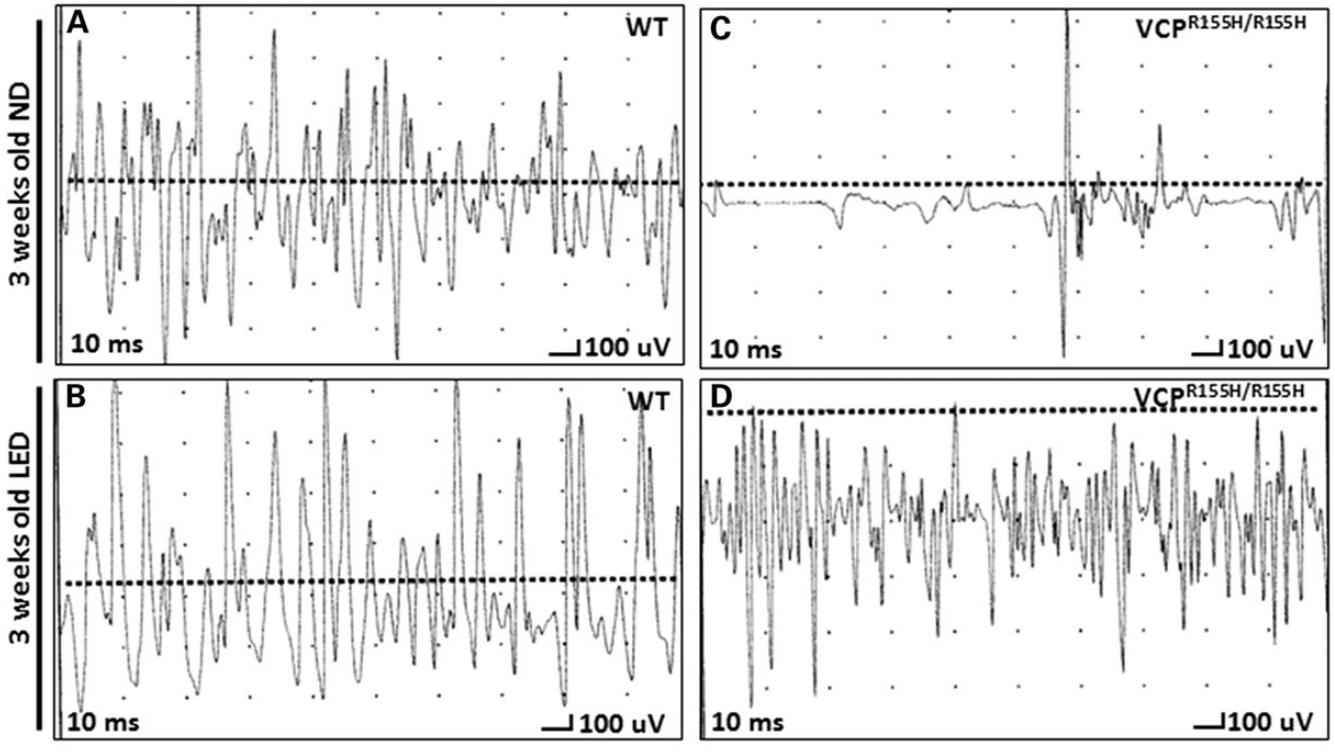

E

Electrodiagnostic (EMG) Measurements	Wild Type Normal Diet	Wild Type Lipid-Enriched Diet	$VCP^{R155H/R155H}$ Normal Diet	$VCP^{R155H/R155H}$ Lipid-Enriched Diet **$p \leq 0.0001$
Thoracic paraspinal	Normal	Normal	Abnormal	Normal
Right tibialis anterior	Normal	Normal	Abnormal	Normal
Right hamstrings	Normal	Normal	Abnormal	Normal
Right medial gastrocnemius	Normal	Normal	Abnormal	Normal
Left tibialis anterior	Normal	Normal	Abnormal	Normal
Left hamstrings	Normal	Normal	Abnormal	Normal
Left medial gastrocnemius	Normal	Normal	Abnormal	Normal

Figure 2. EMG analysis of quadriceps in $VCP^{R155H/R155H}$ and WT animals on normal and LEDs. EMG data of (**A**) WT animals and (**C**) $VCP^{R155H/R155H}$ animals on a ND at 3 weeks of age, and (**B**) WT animals and (**D**) $VCP^{R155H/R155H}$ animals on a LED at 3 weeks of age. Each graph shows a representative from three animals analyzed. (**E**) EMG muscle measurements (bilateral tibialis anterior, bilateral hamstrings, bilateral medial gastrocnemius and unilateral thoracic paraspinal muscles) of 3-week-old WT and $VCP^{R155H/R155H}$ animals on ND versus LEDs. **denotes a statistical significance of $P \leq 0.0001$.

the $VCP^{R155H/R155H}$ animals versus their WT littermates. At 3 weeks of age, the $VCP^{R155H/R155H}$ mice on a LED showed nuclear TDP-43 expression, which is suggestive of a reduced pathological phenotype (Fig. 3G and H). Western blot and densitometric analyses of ubiquitin, LC3-I/II, p62 and TDP-43 confirmed these significant findings in the WT and $VCP^{R155H/R155H}$ animals (Fig. 3I). Remarkably, a decrease in LC3-I expression was observed followed by an increased conversion to LC3-II. Distribution levels of VCP expression were comparable in quadriceps muscles of WT and $VCP^{R155H/R155H}$ animals (data not shown).

Mitochondrial complex analysis in $VCP^{R155H/R155H}$ mice

To examine the effects of LED on the mitochondrial complexes of WT and homozygous $VCP^{R155H/R155H}$ animals, we performed mitochondrial assays. Identification of oxidative and non-oxidative fibers is used in assessing mitochondrial pathology. Trichrome Gomori staining revealed mitochondrial myopathy ('ragged red fibers' and fiber degeneration) in the $VCP^{R155H/R155H}$ mice on the ND, but not in the $VCP^{R155H/R155H}$ mice on the LED (Fig. 4A and B). Compared with 3-week-old WT littermates on an ND which depicted a normal 'checkered' pattern, nicotinamide adenine dinucleotide (NADH) staining of homozygous $VCP^{R155H/R155H}$ mice quadriceps on the ND revealed a decrease in Type II fibers (lighter fibers), suggestive of neuropathic myopathy (Fig. 4C). $VCP^{R155H/R155H}$ homozygous mice on the LED revealed an increase in Type II fibers, suggestive of a reduction in neuropathic myopathy on a LED (Fig. 4D). Compared with 3-week-old WT littermates on a ND (Fig. 4E), succinic dehydrogenase (SDH) staining revealed a significant increase in positive SDH Type I fibers in the $VCP^{R155H/R155H}$ mice fed a LED, suggestive of a higher oxidative capacity (Fig. 4F). Generation of lipid granules was not

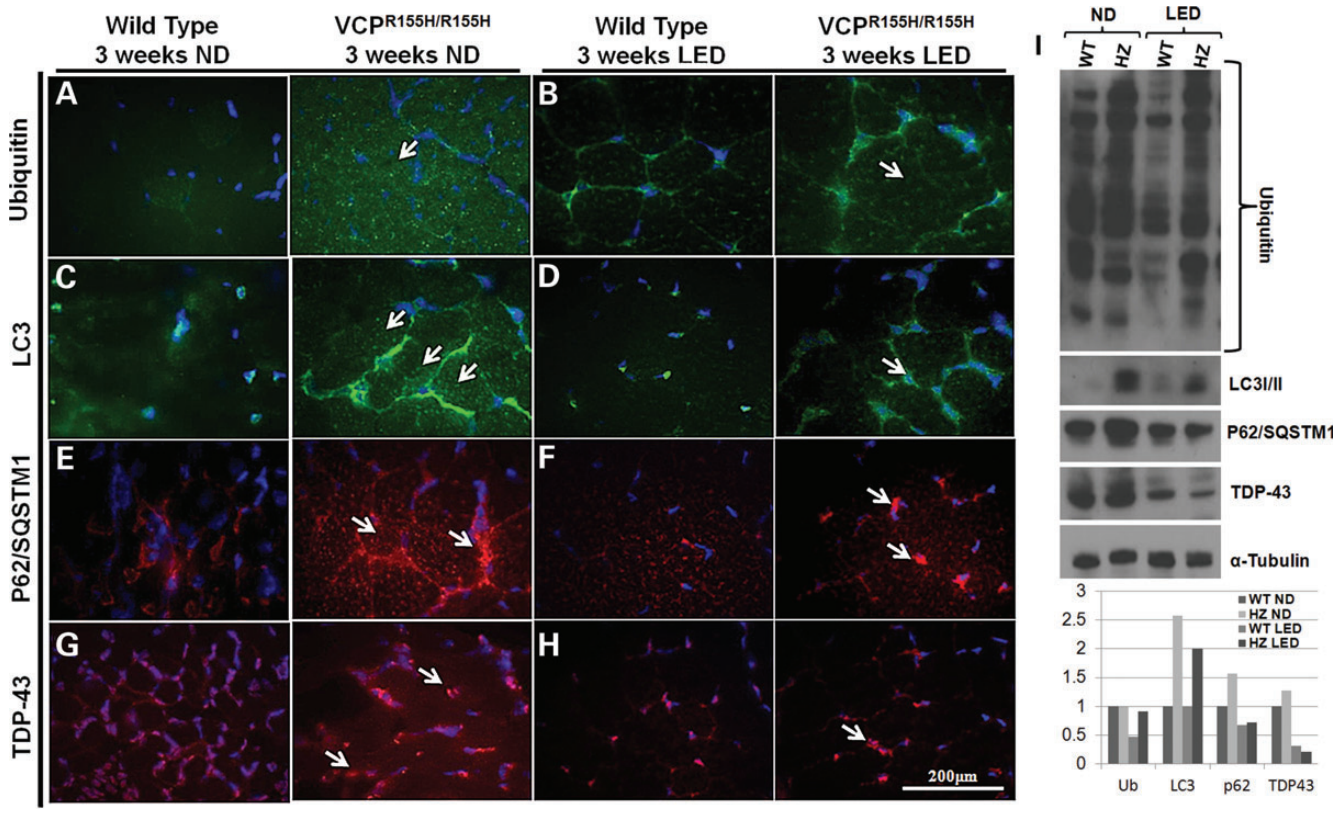

Figure 3. Autophagy is stimulated in the quadriceps of WT and VCP$^{R155H/R155H}$ mice on a LED. Quadriceps muscles from 3-week-old WT and VCP$^{R155H/R155H}$ mice on a (**A**, **C**, **E** and **G**) ND and (**B**, **D**, **F** and **H**) LED were stained with anti-ubiquitin, LC3, p62 and TDP-43-specific antibodies, respectively (shown by arrows). Nuclei were stained with DAPI (magnification: 630×). (**I**) Western blot expression analysis of autophagy proteins including ubiquitin, LC3-I/II, p62 and TDP-43. Alpha-tubulin was used as a positive control. Densitometric analysis of western blot bands as shown in a bar graph. The number of mice analyzed per experiment is 5–6.

noticeable in WT mice by Oil Red O staining; however, the VCP$^{R155H/R155H}$ quadriceps of ND mice showed small lipid granules in a scattered pattern (Fig. 4G). WT and VCP$^{R155H/R155H}$ mice on the LED did not reveal lipid accumulation (Fig. 4H).

LED prevents Paget-like lesions in VCP$^{R155H/R155H}$ mice and kyphosis

To further characterize the bone pathology, we analyzed WT and VCP$^{R155H/R155H}$ mice on a LED versus ND at 3 weeks of age by microtomography (microCT) imaging. To examine the effects of LED on the kyphosis in the WT and homozygous VCP$^{R155H/R155H}$ animals, we examined the cervical and thoracic spine curvatures as measured by the angles. The curvatures of the thoracic and cervical spines were significantly reduced in the 3-week-old VCP$^{R155H/R155H}$ mice on the LED when compared with the 3-week-old VCP$^{R155H/R155H}$ mice on the ND (P values for thoracic kyphosis $P \leq 0.007$ and cervical kyphosis $P \leq 0.005$) (Fig. 5 and Table 1). Kyphosis was also observed in the 4-month- and 9-month-old VCP$^{R155H/R155H}$ mice on the LED when compared with the WT mice (Fig. 5A–H) suggestive of the progressive neuromuscular pathology. Close inspection of the long hind limb bones revealed lucencies of the proximal tibiae in the VCP$^{R155H/R155H}$ mice on the ND at 3 weeks of age, suggestive of PDB (Fig. 5J) (25). Remarkably, the LED significantly reduced the number of Paget-like lesions in the VCP$^{R155H/R155H}$ mice at 3 weeks of age (0.005) (Fig. 5L and Q). However, progressive enlarged and bony lytic lesions were observed in most of the VCP$^{R155H/R155H}$ mice at 4 months and 9 months of age on the LED diet suggesting that PDB cannot be entirely prevented (Fig. 5N, P and Q right panels, arrows). VCP$^{R155H/R155H}$ mice on an ND at 4- and 9-months of age could not be compared as they do not survive past 21 days of age.

Targeted lipidomic analyses of the VCP$^{R155H/R155H}$ and WT animals

To investigate the metabolic consequences of VCP-associated disease on the normal and LEDs, we performed a targeted lipidomic analysis on skeletal muscle quadriceps and liver tissues in homozygous VCP$^{R155H/R155H}$ and WT mice. The first notable result of our analyses was that muscle tissue of VCP$^{R155H/R155H}$ mice on an ND contained significantly higher levels of non-esterified palmitic acid (Fig. 6A; Supplementary material, Table S1), a known lipotoxic fatty acid. Importantly, the amount of palmitic acid in VCP$^{R155H/R155H}$ mice was significantly reduced by the LED, with the levels approaching the levels found in WT mice fed an ND. VCP$^{R155H/R155H}$ mice fed an ND also displayed elevated levels of ceramide (d18:1/16:0) compared with WT mice fed the same diet. As seen with palmitic acid, exposure to the LED normalized ceramide levels in VCP$^{R155H/R155H}$ mice (Fig. 6B). Palmitic acid, but not ceramide (d18:1/16:0), was also

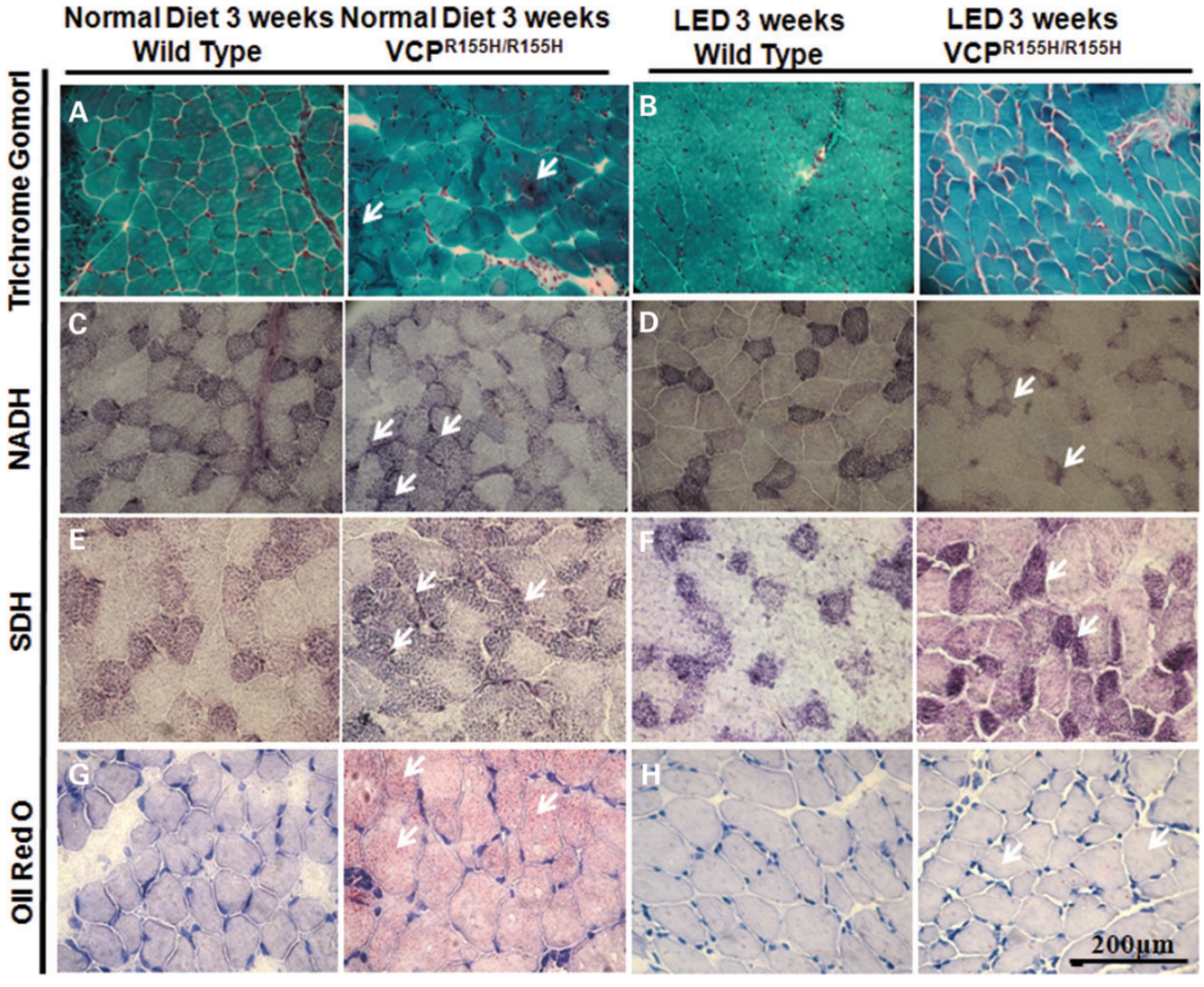

Figure 4. Mitochondrial enzyme analysis of the WT and $VCP^{R155H/R155H}$ mouse quadriceps muscles on normal and LEDs. Quadriceps muscles from WT and $VCP^{R155H/R155H}$ mice at 3 weeks of age on (**A**) normal and ('ragged red' fibers and fiber degeneration shown by arrows) and (**B**) LEDs were stained with Gomori Trichrome. Quadriceps muscles from WT and $VCP^{R155H/R155H}$ mice at 3 weeks of age on a (**C**) normal and (**D**) LEDs stained with NADH antibody. Quadriceps muscles from WT and $VCP^{R155H/R155H}$ mice at 3 weeks of age on a (**E**) normal and (**F**) LEDs stained with SDH antibody. Quadriceps muscles from WT and $VCP^{R155H/R155H}$ mice at 3 weeks of age on a (**G**) normal and (**H**) LEDs stained with Oil Red O (Magnification: 400×). The number of mice analyzed per experiment is 5–6.

significantly elevated in the liver of $VCP^{R155H/R155H}$ mice fed an ND, relative to the WT mice (Fig. 6C and D). Moreover, TUNEL analysis showed that exogenous ceramide caused a dose-dependent stimulation of apoptosis in fibroblasts from both $VCP^{R155H/R155H}$ and WT mice (Fig. 6E). Overall, these results indicate that systemic alterations in lipid metabolism may underlie the muscle-specific pathology of $VCP^{R155H/R155H}$ knock-in mice. Thus, feeding with LED is sufficient to normalize the lipid abnormalities, further highlighting their pathological relevance.

DISCUSSION

Despite intense investigations, the discovery of effective novel therapeutics and the disease mechanisms underlying VCP-associated myopathies and neurodegenerative disorders remain elusive. The homozygous $VCP^{R155H/R155H}$ mouse model has an accelerated pathology of the muscle, brain and spinal cord and is lethal typically by 21 days of age (26). High-fat diets provide powerful therapeutic platforms for many diverse neurological disorders including Alzheimer's disease (AD), Parkinson's disease, neural trauma, autism, multiple sclerosis, ALS and epilepsies (27–32). Studies have also demonstrated amelioration of neurological deficits, regulation of autophagy flux, skeletal muscle homeostasis and a reduction of mitochondrial myopathies in mice fed a LED (33–35). One study examined the effects of ketogenic diet (KD) on the features of children with drug therapy-resistant epilepsy and discovered that KD significantly reduces the frequency of epileptic discharges and demonstrates good clinical efficacy (36). Similarly,

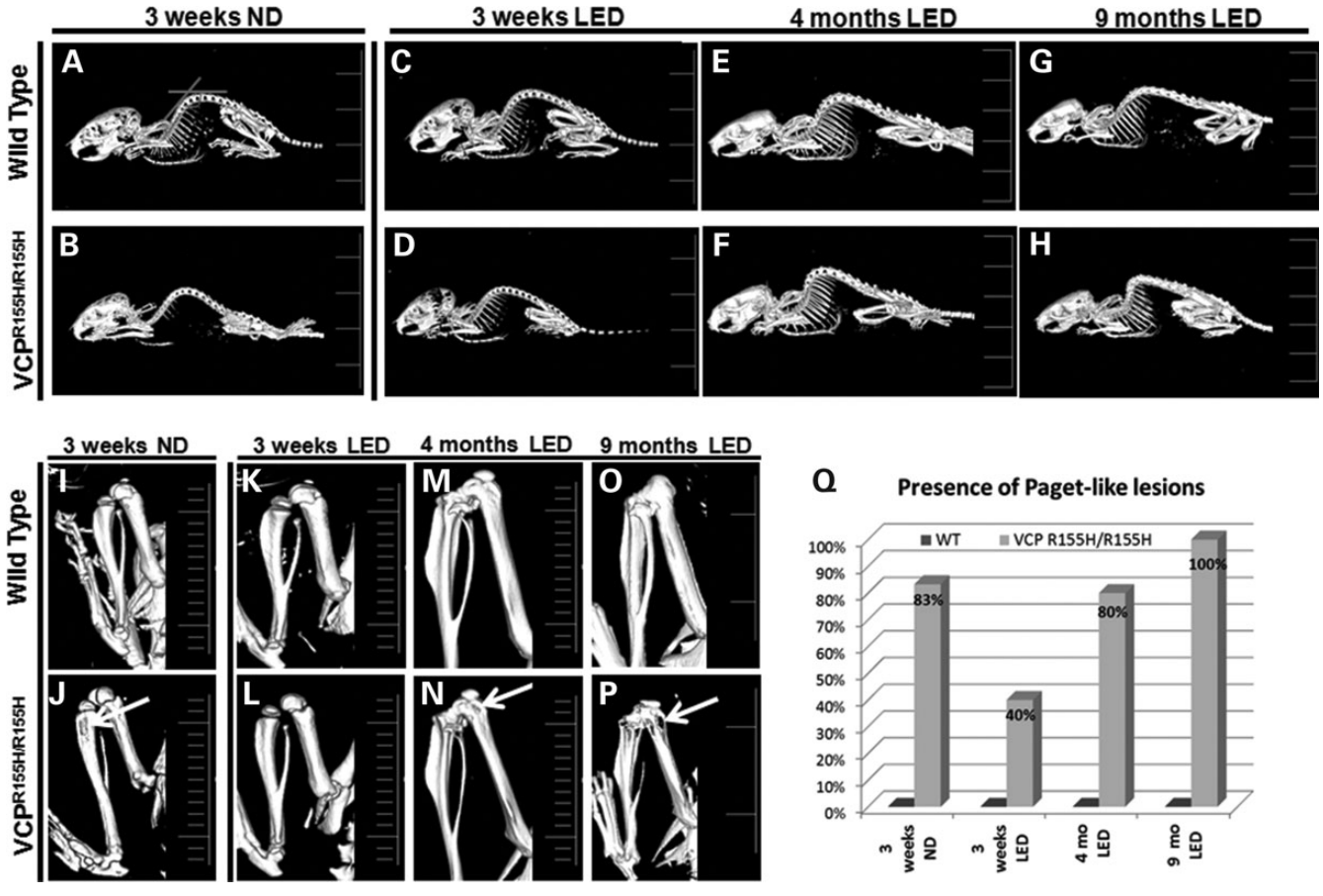

Figure 5. MicroCT analysis of hind limb bones in WT and $VCP^{R155H/R155H}$ animals on normal and LEDs. (**A**–**H**) MicroCT images showed thoracic and cervical kyphosis of the $VCP^{R155H/R155H}$ mice at 3 weeks, 4 months and 9 months of age. (**I**–**P**) Close inspection of the long hind limb bones revealed lucencies of the proximal tibiae (shown by arrows) in the 3-week-old $VCP^{R155H/R155H}$ mice on an ND and in the 4-month and 9-month-old $VCP^{R155H/R155H}$ mice on the LED. (**Q**) Quantification of Paget-like lesions from ND and LED WT and $VCP^{R155H/R155H}$ animals at 3 weeks, 4 months and 9 months of age. The number of mice analyzed per experiment is 5–6.

another study examining the effects of KD in patients with argininosuccinate lyase deficiency showed no metabolic derangement and is well tolerated in patients treated with a protein restriction (37). In animal models, several reports have demonstrated the neuroprotective properties of the KD (38,39).

In our attempts to understand the progressive course of the $VCP^{R155H/R155H}$ homozygous phenotype, we monitored the weights, muscle strength and quadriceps muscles in animals on normal and LEDs. Most significantly, we were able to reverse the lethal phenotype by 21 days of age and increase the survival rate in $VCP^{R155H/R155H}$ mice by placing pregnant dams on LED. Homozygous $VCP^{R155H/R155H}$ animals demonstrated normal histology of quadriceps muscle fibers at 3 weeks of age and a slower progression of the disease in the survivors on the LED. A significant improvement in muscle strength measurements in the $VCP^{R155H/R155H}$ animals on the LED versus their age-matched littermates placed on the ND was observed. However, the LED did not prevent fatal progression of the disease in the mutant $VCP^{R155H/R155H}$ mice. The LED regimen did not show any detrimental effects on $VCP^{R155H/R155H}$ mice which did not develop obesity, whereas there was significant weight gain in WT mice, mostly accumulated as layers of adipose tissue. The $VCP^{R155H/R155H}$ mutant mice on a ND depicted a lower number of SDH- and NADH-stained Type II fibers and higher mitochondrial density in their muscle tissues, whereas the $VCP^{R155H/R155H}$ mutant mice on LED showed amelioration of the mitochondrial pathology.

Literature has suggested that high-fat diet ameliorates neurological deficits caused by defective lipid metabolism (33). A report by Koga *et al*. (2010) has demonstrated altered lipid composition/content inhibits autophagosome/lysosome vesicular fusion (40). One of the major effects observed in the ND is lipid accumulation in skeletal muscle, which may possibly be due to an imbalance between energy intake and expenditure caused by a number of transduction pathways. These signaling cascades could possibly lead to increased uptake of fatty acids into the muscle from circulation or defective muscle mitochondrial metabolism (35). In this report, analyses performed on quadriceps muscles of 3-week-old homozygous mice revealed significant differences in the histological, biochemical and metabolic lipidomic parameters. Compared with WT animals on a ND, the homozygous $VCP^{R155H/R155H}$ animals had an increase in uptake of higher free fatty acids (16:0, 18:1 and 18:2) in the quadriceps muscles. These increased fatty acids, especially

Table 1. Thoracic and cervical kyphosis in WT and $VCP^{R155H/R155H}$ animals

Diet	Age	Angle (°) thoracic kyphosis WT	$VCP^{R155H/R155H}$	*P* (WT versus $VCP^{R155H/R155H}$)	Angle (°) cervical kyphosis WT	$VCP^{R155H/R155H}$	*P* (WT versus $VCP^{R155H/R155H}$)
ND	3 weeks	146.5 ± 5.2 ($n = 4$)	120.75 ± 4.4 ($n = 4$)	<0.0001*	128.25 ± 5.5 ($n = 4$)	103.5 ± 5.5 ($n = 4$)	<0.0001*
LED	3 weeks	144.25 ± 3.8 ($n = 5$)	130 ± 1.5 ($n = 4$)	<0.003*	126.25 ± 2.0 ($n = 5$)	116 ± 2.0 ($n = 4$)	<0.0001*
LED	4 months	141.6 ± 1.4 ($n = 5$)	119 ± 2.2 ($n = 5$)	<0.0001*	113 ± 6.4 ($n = 5$)	106.25 ± 4.7 ($n = 5$)	<0.094
LED	9 months	145.6 ± 0.8 ($n = 4$)	111 ± 2.5 ($n = 4$)	<0.0001*	107.3 ± 5.8 ($n = 4$)	98.6 ± 0.8 ($n = 4$)	<0.025*

*denotes a statistical significance of $P < 0.0001$.

palmitic acid (16:0) and ceramide (d18:1/16:0) within the quadriceps and liver tissues, suggest lipotoxicity, compromised skeletal muscle homeostasis, impaired mitochondrial metabolism and autophagy. However, maternal and early feeding of pups with a LED significantly resulted in a reduction of palmitic acid and ceramide levels in both quadriceps and liver of $VCP^{R155H/R155H}$ animals, restoring levels to almost those seen in WT mice. A possible explanation for the improved pathology is that the LED results in a decrease in palmitic acid and ceramide levels, which are known to cause lipotoxicity, apoptosis, necrotic cell death and autophagy. Palmitic acid is known to induce cellular dysfunction, cell death and lysosomal dysfunction in hepatocytes, cardiomyocytes, pancreatic beta cells and several other cell types (41). Studies have demonstrated that palmitate causes multiple ER stress responses and early induction of the Akt pathway. Palmitate modulates intracellular signaling causing cellular stress leading to increased autophagic and apoptotic signaling cascades (41). Similarly, ceramides are sphingosine-based lipid messengers known to interfere with insulin growth factor-1 (IGF-1)/insulin signaling, thereby resulting in decreased expression and activation of Akt, leading to several consequences (42–44). Increased ceramide production may contribute to myofiber atrophy, whereby ceramide inhibits IGF-1 induced protein synthesis and differentiation, in turn inhibiting muscular growth and repair mechanisms. *In vitro*, ceramide inhibits IGF-1 protein synthesis and expression of MyoD and myogenin, thereby resulting in reduced myoblast differentiation and fusion into myotubes (45). In myotubes, ceramide induces apoptosis, oxidative stress and mitochondrial dysfunction. Ceramide in brains may lead to Alzheimer's disease and motor neuron death in ALS (46,47). Here, we provide evidence that these lipids possibly act as culprits in our VCP mouse model as evidenced by the ceramide treatment in fibroblasts. *In vitro* studies performed on the homozygote $VCP^{R155H/R155H}$ and WT fibroblasts showed that increased levels of ceramide resulted in dose-dependent apoptosis, with an increased effect in the homozygotes. It is possible that increased ceramide levels observed in the homozygote quadriceps on a ND may be contributing to the muscle and bone pathology. Collectively, the ability of the LED to reduce ceramide levels in $VCP^{R155H/R155H}$ mice suggests a potentially protective effect against fatty acid-induced lipotoxicity and therapeutic effects by allowing mechanisms of repair and growth of skeletal muscle tissue. It seems likely that other mechanistic pathways, such as modification of autophagy, may also play a role in the prolonged survival of the homozygous mice.

Autophagy is a critical catabolic process necessary for cell growth, development and homeostatic levels of cellular products, and more recently a role in regulating glucose metabolism has been identified. Evidence suggests a molecular link between autophagy and cellular metabolism (48,49) and thus, is important in times of survival during fasting and for reprograming of cell metabolism (49). Studies have demonstrated the importance of autophagy in maintaining protein homeostasis and quality control of cellular milieu. However, mechanisms underlying neurodegeneration owing to autophagy dysfunction remain unknown. In our study, the 3-week-old $VCP^{R155H/R155H}$ homozygous animals on a LED demonstrated decreased expression levels of p62/SQSTM1, ubiquitin and LC3 autophagy intermediates in muscle compared with 3-week-old $VCP^{R155H/R155H}$ homozygous littermates on a ND, thereby suggesting an improvement in the functionality of the autophagic cascade, an important feature of VCP-associated disease.

Paget's disease of bone is characterized by disorganized architecture, reduced mechanical strength and focal abnormalities of increased bone turnover affecting one or more skeletal sites (50,51). There is increasing evidence that abnormalities in autophagy may contribute to PDB pathogenesis in a mouse model (52). Linkage and positional cloning studies provide strong evidence that the mutations in the gene encoding p62/*SQSTM1* causes Paget's disease of bone in patients, thereby identifying p62 as a critical player in osteoclast signaling in PDB (53) and as a cause for ALS (54). Remarkably, the LED reduced the formation of Paget-like lesions in the 3-week-old $VCP^{R155H/R155H}$ mutant mice compared with their littermates on the ND. Studies are underway to clarify the association between LED and prevention/therapeutic effect of PDB.

In this report, we established that the effect of a LED reversed the lethal phenotype of the $VCP^{R155H/R155H}$ animals and significantly improved muscle and bone pathology, motor activity as well as myopathic and mitochondrial staining at 3 weeks of age. Our findings further confirm a link between autophagy, fatty acid metabolism and cellular homeostasis. We hypothesize that the LED counterbalances the detrimental effects of the *VCP* R155H mutation by altering free fatty acid levels involved in various signaling mechanisms critical for survival. Further elucidation of the importance of fatty acid profiles and its connection to autophagic and metabolic signaling pathways could provide insights for future translational applications. Further studies are underway to analyze the brain and spinal cord pathologies of our *in vivo* model, which offers the prospect of understanding the translational cellular/molecular mechanisms and

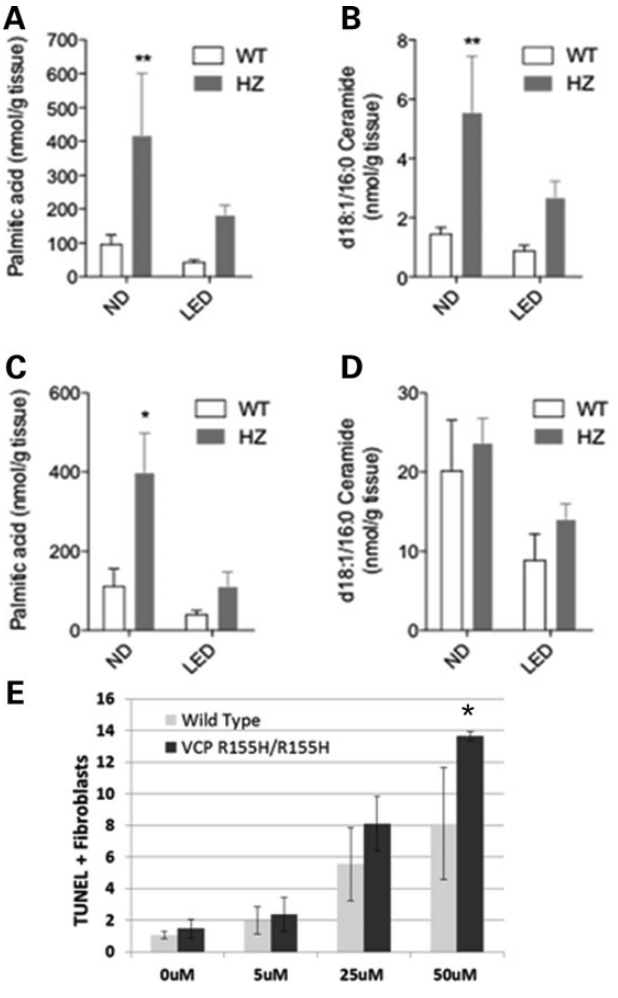

Figure 6. Lipid analyses of quadriceps muscles and livers from WT and $VCP^{R155H/R155H}$ animals on normal and LEDs. (**A** and **B**) Levels of non-esterified palmitic acids (A, $n = 4–6$) and d18:1/16:0 ceramides (B, $n = 7–9$) in the quadriceps of WT and $VCP^{R155H/R155H}$ mice on the normal versus LEDs were determined by using liquid chromatography–mass spectrometry (LC–MS). (**C** and **D**) Levels of non-esterified palmitic acids (C) or d18:1/16:0 ceramide (D) in the liver of WT and $VCP^{R155H/R155H}$ mice on the normal versus LEDs were determined using LC–MS ($n = 4–6$). (**E**) Percentage of TUNEL+ fibroblasts from WT and $VCP^{R155H/R155H}$ animals treated for 24 h with increasing ceramide concentrations. Experiments were done in triplicate.

the development of dietary novel drugs to treat patients with VCP-associated neurodegenerative diseases.

MATERIALS AND METHODS

Ethics statement and animal models

All experiments were done with the approval of the Institutional Animal Care and Use Committee (IACUC Protocol #2007-2716-2), and in accordance with the guidelines established by the National Institutes of Health. Animals were housed at University of California, Irvine vivarium and maintained under constant temperature (22°C) and humidity with a controlled 12:12-h light–dark cycle. Mice were euthanized by CO_2 inhalation followed by cervical dislocation in all experiments.

Normal and lipid-enriched diet regimens

VCP heterozygote pregnant dams were chosen for this study and placed on the *ad libitum* LED (2019× Teklad Rodent Diets, Harlan Laboratories, Inc., Madison, WI, USA) or standard ND (2020×) (Supplementary material, Table S2). At weaning, the animals were separated and continued to receive the same diet. The homozygous and WT animals were both on a C57BL/6J background. All experiments performed in this study were checked genetically and identified by genotyping (Transnetyx, Inc., Cordova, TN, USA).

Weight and grip strength measurement studies

Weights of the $VCP^{R155H/R155H}$ and WT animals on the ND and LED were measured on a weekly basis to follow body mass development. Muscle strength of the forelimbs was measured using a Grip Strength Meter apparatus (TSE Systems Gmbh, Hamburg, Germany) as described previously (55).

Electromyography measurements

Neurophysiological terminal EMG recordings were performed *in vivo* in the limbs of 3-week-old $VCP^{R155H/R155H}$ and WT mice under Ketamine-Xylazine anesthesia. The following muscles were examined: bilateral tibialis anterior, bilateral hamstrings and bilateral medial gastrocnemius muscles, and unilateral thoracic paraspinal muscles. Patterns of insertional and spontaneous activity were noted in all these muscles along with pattern of motor unit potentials evoked by movement of limbs caused by noxious stimuli given to the footpads. All recordings were made using a Nicolet Viking Quest portable EMG machine (Cardinal Health, Hudson, WI, USA).

MicroCT imaging

MicroCT scans were performed by scanning 3-week-, 4-month- and 9-month-old WT and $VCP^{R155H/R155H}$ mice with a large area CT camera. The reconstructed microCT images were analyzed and trabecular structural parameters were determined using the Inveon Multimodality 3D Visualization software.

Histological and immunofluorescence analysis

Quadriceps muscles from 3-week-, 4-month- and 9-month-old $VCP^{R155H/R155H}$ and WT mice were harvested. Hematoxylin and Eosin (H&E) staining was performed using routine methods and analyzed by light microscopy (Carl Zeiss, Thornwood, NY, USA) (55). For immunohistochemical analyses, sections were stained with TDP-43, ubiquitin, VCP, LC3-I/II and p62/*SQSTM1*. All primary antibodies were purchased from Abcam (Cambridge, MA, USA). Subsequently, sections were washed with 1× phosphate-buffered saline (PBS) and incubated with fluorescent-conjugated secondary antibodies (Sigma–Aldrich, St. Louis, MO, USA) for 1 h at room temperature and mounted with DAPI-containing mounting media (Vector Laboratories, Inc., Burlingame, CA, USA) and analyzed by fluorescence microscopy.

Assessment of mitochondrial markers

Histochemical analyses were performed by Gomori Trichrome staining and activity levels with SDH (Sigma–Aldrich) and NADH (Sigma–Aldrich) were performed on quadriceps muscles from the $VCP^{R155H/R155H}$ and WT mice as previously described (56). Quadriceps cross-sections were incubated with SDH or NADH for 2 h in the incubator at 37°C. To check for lipid deposits, quadriceps sections were stained in Oil Red O solution for 10 min, rinsed in 60% isopropanol, counterstained for 1 min in Harris' hematoxylin followed by a 2 min blueing step. Following incubation, slides were cooled off for 5 min at room temperature and mounted with Aquamount (Thermo Scientific, Pittsburgh, PA, USA). The staining intensity was evaluated using light microscopy.

Protein extraction and analysis

Quadriceps muscle samples from 3-week-old $VCP^{R155H/R155H}$ and WT animals were harvested and extracted using the NE-PER Nuclear and Cytoplasmic Extraction Kit (Thermo Scientific). Protein concentrations were determined using the Nanodrop and separated on Bis-Tris 4–12% Nu-PAGE gels (Invitrogen Life Technologies, Inc., Carlsbad, CA, USA). Expression levels of proteins were analyzed by western blotting using VCP (Thermo Scientific), TDP-43, p62/*SQSTM1*, LC3-I/II and ubiquitin-specific antibodies. Equal protein loading was confirmed by α-tubulin or β-actin antibodies (Santa Cruz Biotechnology, Santa Cruz, CA, USA) staining.

Lipidomics analysis

Lipids were extracted from flash-frozen quadriceps muscles and livers of 3-week-old $VCP^{R155H/R155H}$ and WT animals on ND and LED as previously described (57). Additional lipidomics methodology is described in Supplementary material, Table S1.

In Vitro ceramide treatment

Fibroblast cultures were prepared from skin dissected from $VCP^{R155H/R155H}$ and WT mice fed a ND. Briefly, for fibroblast cultures, the skin was washed with PBS and cut into 5- to 10-skin pieces and put in the center of a 35-mm culture dish. A coverslip was placed on the skin specimens with a few drops of DMEM. Cells were grown in humidified 5% CO_2 at 37°C incubator in DMEM supplemented with 10% fetal bovine serum. Differentiation medium was not used in these experiments. The fibroblast outgrowth was monitored every 3 to 4 days at which point the medium was changed. At 60% confluency, cells were seeded onto chamber slides (Fisher Scientific, Pittsburgh, PA, USA) and treated with 0, 5, 25 and 50 μM concentrations of C-8 ceramide (Cayman Chemical, Ann Arbor, MI, USA) for 24 h. To measure apoptosis after 24 h, TUNEL assay (Promega, Madison, WI, USA) was performed as per manufacturer's instructions. Briefly, cells were fixed in 4% paraformaldehyde for 25 min at 4°C, washed in PBS for 5 min and permeabilized with 20 μg/ml proteinase K solution and 0.2% Triton X-100 for 10 min at room temperature. Cells were then washed in PBS for 5 min, and 100 μl of equilibration buffer was added for 10 min. The cells were labeled with 50 μl of TdT reaction mix and incubated for 60 min at 37°C in a humidified chamber. Stop reaction was added for 15 min after which the cells were washed, counterstained and prepared for analysis. The percentage of TUNEL positive cells was calculated by counting all cells and TUNEL+ cells per chamber. These experiments are representative of triplicates.

Statistical analysis

Means were used as summary statistics for all experiments. We compared the above studies—including weights, activity, immunohistological and *in vitro* studies—among ND- and LED-fed $VCP^{R155H/R155H}$ and WT mice using mixed model analysis of variance and pair-wise *t*-tests. For EMG studies, statistical results were obtained using the chi-squared test. For lipidomics and TUNEL+ cell analyses, results are expressed as means ± SEM and significance was determined using two-tailed Student's *t*-test or two-way ANOVA with Bonferroni post-test.

SUPPLEMENTARY MATERIAL

Supplementary Material is available at *HMG* online.

ACKNOWLEDGEMENTS

We thank Drs. Cristian Constantinescu and Mohammad Reza Mirbolooki for technical assistance with the MicroCT. We also thank Dr. Kathryn Osann for providing statistical guidance for these experiments and Dr. Manaswitha Khare for generation of the Kaplan–Meier survival curve. We acknowledge Drs. Giles Watts and Hicham Drissi for their expertise in bone pathology. The technical assistance of J. Lockney is also acknowledged. The contribution of the Agilent Technologies/University of California, Irvine Analytical Discovery Facility, Center for Drug Discovery is gratefully acknowledged.

Conflict of Interest statement. None declared.

FUNDING

This work was supported by National Institutes of Health (NIH) grant R21 AR063360 and Muscular Dystrophy Association (MDA) funding to V.E.K. and RC2 DA028902-NIH funding to D.P.

REFERENCES

1. Kimonis, V.E., Kovach, M.J., Waggoner, B., Leal, S., Salam, A., Rimer, L., Davis, K., Khardori, R. and Gelber, D. (2000) Clinical and molecular studies in a unique family with autosomal dominant limb-girdle muscular dystrophy and Paget disease of bone. *Genet. Med.*, **2**, 232–241.
2. Kovach, M.J., Ruiz, J., Kimonis, K., Mueed, S., Sinha, S., Higgins, C., Elble, S., Elble, R. and Kimonis, V.E. (2001) Genetic heterogeneity in autosomal dominant essential tremor. *Genet. Med.*, **3**, 197–199.
3. Nalbandian, A., Donkervoort, S., Dec, E., Badadani, M., Katheria, V., Rana, P., Nguyen, C., Mukherjee, J., Caiozzo, V., Martin, B. *et al.* (2011) The multiple faces of valosin-containing protein-associated diseases: inclusion body myopathy with Paget's disease of bone, frontotemporal dementia, and amyotrophic lateral sclerosis. *J. Mol. Neurosci.*, **45**, 522–531.
4. Watts, G.D., Thorne, M., Kovach, M.J., Pestronk, A. and Kimonis, V.E. (2003) Clinical and genetic heterogeneity in chromosome 9p associated hereditary inclusion body myopathy: exclusion of GNE and three other candidate genes. *Neuromuscul. Disord.*, **13**, 559–567.

5. Kimonis, V.E., Mehta, S.G., Fulchiero, E.C., Thomasova, D., Pasquali, M., Boycott, K., Neilan, E.G., Kartashov, A., Forman, M.S., Tucker, S. *et al.* (2008) Clinical studies in familial VCP myopathy associated with Paget disease of bone and frontotemporal dementia. *Am. J. Med. Genet.*, **146**, 745–757.
6. Watts, G.D., Wymer, J., Kovach, M.J., Mehta, S.G., Mumm, S., Darvish, D., Pestronk, A., Whyte, M.P. and Kimonis, V.E. (2004) Inclusion body myopathy associated with Paget disease of bone and frontotemporal dementia is caused by mutant valosin-containing protein. *Nat. Genet.*, **36**, 377–381.
7. Kimonis, V.E., Fulchiero, E., Vesa, J. and Watts, G. (2008) VCP disease associated with myopathy, paget disease of bone and frontotemporal dementia: Review of a unique disorder. *Biochim. Biophys. Acta*, **1782**, 744–748.
8. Nalbandian, A., Ghimbovschi, S., Radom-Aizik, S., Dec, E., Vesa, J., Martin, B., Knoblach, S., Smith, C., Hoffman, E. and Kimonis, V.E. (2012) Global gene profiling of VCP-associated inclusion body myopathy. *Clin. Transl. Sci.*, **5**, 226–234.
9. Ju, J.S., Fuentealba, R.A., Miller, S.E., Jackson, E., Piwnica-Worms, D., Baloh, R.H. and Weihl, C.C. (2009) Valosin-containing protein (VCP) is required for autophagy and is disrupted in VCP disease. *J. Cell Biol.*, **187**, 875–888.
10. Vesa, J., Su, H., Watts, G.D., Krause, S., Walter, M.C., Martin, B., Smith, C., Wallace, D.C. and Kimonis, V.E. (2009) Valosin containing protein associated inclusion body myopathy: abnormal vacuolization, autophagy and cell fusion in myoblasts. *Neuromuscul. Disord.*, **19**, 766–772.
11. Lee, H.S., Daniels, B.H., Salas, E., Bollen, A.W., Debnath, J. and Margeta, M. (2012) Clinical utility of LC3 and p62 immunohistochemistry in diagnosis of drug-induced autophagic vacuolar myopathies: a case-control study. *PLoS One*, **7**, e36221.
12. Malicdan, M.C. and Nishino, I. (2012) Autophagy in lysosomal myopathies. *Brain Pathol.*, **22**, 82–88.
13. Shea, L. and Raben, N. (2009) Autophagy in skeletal muscle: implications for Pompe disease. *Int. J. Clin. Pharmacol. Ther.*, **47** (Suppl 1), S42–S47.
14. Lunemann, J.D., Schmidt, J., Dalakas, M.C. and Munz, C. (2007) Macroautophagy as a pathomechanism in sporadic inclusion body myositis. *Autophagy*, **3**, 384–386.
15. Goode, A. and Layfield, R. (2010) Recent advances in understanding the molecular basis of Paget disease of bone. *J. Clin. Pathol.*, **63**, 199–203.
16. Hirano, M., Nakamura, Y., Saigoh, K., Sakamoto, H., Ueno, S., Isono, C., Miyamoto, K., Akamatsu, M., Mitsui, Y. and Kusunoki, S. (2013) Mutations in the gene encoding p62 in Japanese patients with amyotrophic lateral sclerosis. *Neurology*, **80**, 458–463.
17. Hiruma, Y., Kurihara, N., Subler, M.A., Zhou, H., Boykin, C.S., Zhang, H., Ishizuka, S., Dempster, D.W., Roodman, G.D. and Windle, J.J. (2008) A SQSTM1/p62 mutation linked to Paget's disease increases the osteoclastogenic potential of the bone microenvironment. *Hum. Mol. Genet.*, **17**, 3708–3719.
18. Laurin, N., Brown, J.P., Morissette, J. and Raymond, V. (2002) Recurrent mutation of the gene encoding sequestosome 1 (SQSTM1/p62) in Paget disease of bone. *Am. J. Hum. Genet.*, **70**, 1582–1588.
19. Rhodes, E.C., Johnson-Pais, T.L., Singer, F.R., Ankerst, D.P., Bruder, J.M., Wisdom, J., Hoon, D.S., Lin, E., Bone, H.G., Simcic, K.J. *et al.* (2008) Sequestosome 1 (SQSTM1) mutations in Paget's disease of bone from the United States. *Calcif. Tissue Int.*, **82**, 271–277.
20. Rubino, E., Rainero, I., Chio, A., Rogaeva, E., Galimberti, D., Fenoglio, P., Grinberg, Y., Isaia, G., Calvo, A., Gentile, S. *et al.* (2012) SQSTM1 mutations in frontotemporal lobar degeneration and amyotrophic lateral sclerosis. *Neurology*, **79**, 1556–1562.
21. Teyssou, E., Takeda, T., Lebon, V., Boillee, S., Doukoure, B., Bataillon, G., Sazdovitch, V., Cazeneuve, C., Meininger, V., Leguern, E. *et al.* (2013) Mutations in SQSTM1 encoding p62 in amyotrophic lateral sclerosis: genetics and neuropathology. *Acta Neuropathol.*, **125**, 511–522.
22. Kim, N.C., Tresse, E., Kolaitis, R.M., Molliex, A., Thomas, R.E., Alami, N.H., Wang, B., Joshi, A., Smith, R.B., Ritson, G.P. *et al.* (2013) VCP is essential for mitochondrial quality control by PINK1/Parkin and this function is impaired by VCP mutations. *Neuron.*, **78**, 65–80.
23. Bartolome, F., Wu, H.C., Burchell, V.S., Preza, E., Wray, S., Mahoney, C.J., Fox, N.C., Calvo, A., Canosa, A., Moglia, C. *et al.* (2013) Pathogenic VCP mutations induce mitochondrial uncoupling and reduced ATP levels. *Neuron*, **78**, 57–64.
24. Nalbandian, A., Llewellyn, K.J., Badadani, M., Yin, H.Z., Nguyen, C., Katheria, V., Watts, G., Mukherjee, J., Vesa, J., Caiozzo, V. *et al.* (2013) A progressive translational mouse model of human valosin-containing protein disease: the VCP(R155H/+) mouse. *Muscle Nerve*, **47**, 260–270.
25. Yin, H.Z., Nalbandian, A., Hsu, C.I., Li, S., Llewellyn, K.J., Mozaffar, T., Kimonis, V.E. and Weiss, J.H. (2012) Slow development of ALS-like spinal cord pathology in mutant valosin-containing protein gene knock-in mice. *Cell Death Dis.*, **3**, e374.
26. Nalbandian, A., Llewellyn, K.J., Kitazawa, M., Yin, H.Z., Badadani, M., Khanlou, N., Edwards, R., Nguyen, C., Mukherjee, J., Mozaffar, T. *et al.* (2012) The homozygote $VCP^{R155H/R155H}$ mouse model exhibits accelerated human VCP-associated disease pathology. *PLoS One*, **7**, e46308.
27. Baranano, K.W. and Hartman, A.L. (2008) The ketogenic diet: uses in epilepsy and other neurologic illnesses. *Curr. Treat Options Neurol.*, **10**, 410–419.
28. Evangeliou, A., Vlachonikolis, I., Mihailidou, H., Spilioti, M., Skarpalezou, A., Makaronas, N., Prokopiou, A., Christodoulou, P., Liapi-Adamidou, G., Helidonis, E. *et al.* (2003) Application of a ketogenic diet in children with autistic behavior: pilot study. *J. Child Neurol.*, **18**, 113–118.
29. Gasior, M., Rogawski, M.A. and Hartman, A.L. (2006) Neuroprotective and disease-modifying effects of the ketogenic diet. *Behav. Pharmacol.*, **17**, 431–439.
30. Jozwiak, S., Kossoff, E.H. and Kotulska-Jozwiak, K. (2011) Dietary treatment of epilepsy: rebirth of an ancient treatment. *Neurol. Neurochir. Pol.*, **45**, 370–378.
31. Siva, N. (2006) Can ketogenic diet slow progression of ALS? *Lancet Neurol.*, **5**, 476.
32. Stafstrom, C.E. and Rho, J.M. (2012) The ketogenic diet as a treatment paradigm for diverse neurological disorders. *Front Pharmacol.*, **3**, 59.
33. Camargo, N., Brouwers, J.F., Loos, M., Gutmann, D.H., Smit, A.B. and Verheijen, M.H. (2012) High-fat diet ameliorates neurological deficits caused by defective astrocyte lipid metabolism. *FASEB J.*, **26**, 4302–4315.
34. Moresi, V., Carrer, M., Grueter, C.E., Rifki, O.F., Shelton, J.M., Richardson, J.A., Bassel-Duby, R. and Olson, E.N. (2012) Histone deacetylases 1 and 2 regulate autophagy flux and skeletal muscle homeostasis in mice. *Proc. Nat. Acad. Sci. USA*, **109**, 1649–1654.
35. Turner, N., Bruce, C.R., Beale, S.M., Hoehn, K.L., So, T., Rolph, M.S. and Cooney, G.J. (2007) Excess lipid availability increases mitochondrial fatty acid oxidative capacity in muscle: evidence against a role for reduced fatty acid oxidation in lipid-induced insulin resistance in rodents. *Diabetes*, **56**, 2085–2092.
36. Li, B., Tong, L., Jia, G. and Sun, R. (2013) Effects of ketogenic diet on the clinical and electroencephalographic features of children with drug therapy-resistant epilepsy. *Exp. Ther. Med.*, **5**, 611–615.
37. Peuscher, R., Dijsselhof, M.E., Abeling, N.G., Van Rijn, M., Van Spronsen, F.J. and Bosch, A.M. (2012) The ketogenic diet is well tolerated and can be effective in patients with argininosuccinate lyase deficiency and refractory epilepsy. *JIMD Reports*, **5**, 127–130.
38. Luan, G., Zhao, Y., Zhai, F., Chen, Y. and Li, T. (2012) Ketogenic diet reduces Smac/Diablo and cytochrome c release and attenuates neuronal death in a mouse model of limbic epilepsy. *Brain Res. Bull.*, **89**, 79–85.
39. Noh, H.S., Kim, Y.S. and Choi, W.S. (2008) Neuroprotective effects of the ketogenic diet. *Epilepsia*, **49** (Suppl 8), 120–123.
40. Koga, H., Kaushik, S. and Cuervo, A.M. (2010) Altered lipid content inhibits autophagic vesicular fusion. *FASEB. J.*, **24**, 3052–3065.
41. Mei, S., Ni, H.M., Manley, S., Bockus, A., Kassel, K.M., Luyendyk, J.P., Copple, B.L. and Ding, W.X. (2011) Differential roles of unsaturated and saturated fatty acids on autophagy and apoptosis in hepatocytes. *J. Pharmacol. Exp. Ther.*, **339**, 487–498.
42. Bruni, P. and Donati, C. (2008) Pleiotropic effects of sphingolipids in skeletal muscle. *Cell Mol. Life Sci.*, **65**, 3725–3736.
43. Buren, J., Lai, Y.C., Lundgren, M., Eriksson, J.W. and Jensen, J. (2008) Insulin action and signalling in fat and muscle from dexamethasone-treated rats. *Arch. Biochem. Biophys.*, **474**, 91–101.
44. Holland, W.L., Brozinick, J.T., Wang, L.P., Hawkins, E.D., Sargent, K.M., Liu, Y., Narra, K., Hoehn, K.L., Knotts, T.A., Siesky, A. *et al.* (2007) Inhibition of ceramide synthesis ameliorates glucocorticoid-, saturated-fat-, and obesity-induced insulin resistance. *Cell Metab.*, **5**, 167–179.
45. Turpin, S.M., Lancaster, G.I., Darby, I., Febbraio, M.A. and Watt, M.J. (2006) Apoptosis in skeletal muscle myotubes is induced by ceramides and is positively related to insulin resistance. *Am. J. Physiol. Endocrinol. Metab.*, **291**, E1341–E1350.
46. Cutler, R.G., Pedersen, W.A., Camandola, S., Rothstein, J.D. and Mattson, M.P. (2002) Evidence that accumulation of ceramides and cholesterol esters

mediates oxidative stress-induced death of motor neurons in amyotrophic lateral sclerosis. *Ann. Neurol.*, **52**, 448–457.
47. Filippov, V., Song, M.A., Zhang, K., Vinters, H.V., Tung, S., Kirsch, W.M., Yang, J. and Duerksen-Hughes, P.J. (2012) Increased ceramide in brains with Alzheimer's and other neurodegenerative diseases. *J. Alzheimers Dis.*, **29**, 537–547.
48. Rabinowitz, J.D. and White, E. (2010) Autophagy and metabolism. *Science*, **330**, 1344–1348.
49. Schiaffino, S., Mammucari, C. and Sandri, M. (2008) The role of autophagy in neonatal tissues: just a response to amino acid starvation? *Autophagy*, **4**, 727–730.
50. Ralston, S.H. (2013) Clinical practice. Paget's disease of bone. *N. Engl. J. Med.*, **368**, 644–650.
51. Ralston, S.H. and Layfield, R. (2012) Pathogenesis of Paget disease of bone. *Calcif. Tissue Int.*, **91**, 97–113.
52. Daroszewska, A., van 't Hof, R.J., Rojas, J.A., Layfield, R., Landao-Basonga, E., Rose, L., Rose, K. and Ralston, S.H. (2011) A point mutation in the ubiquitin-associated domain of SQSMT1 is sufficient to cause a Paget's disease-like disorder in mice. *Hum. Mol. Genet.*, **20**, 2734–2744.
53. Chamoux, E., Couture, J., Bisson, M., Morissette, J., Brown, J.P. and Roux, S. (2009) The p62 P392L mutation linked to Paget's disease induces activation of human osteoclasts. *Mol. Endocrinol.*, **23**, 1668–1680.
54. Fecto, F., Yan, J., Vemula, S.P., Liu, E., Yang, Y., Chen, W., Zheng, J.G., Shi, Y., Siddique, N., Arrat, H. *et al.* (2011) SQSTM1 mutations in familial and sporadic amyotrophic lateral sclerosis. *Arch. Neurol.*, **68**, 1440–1446.
55. Badadani, M., Nalbandian, A., Watts, G.D., Vesa, J., Kitazawa, M., Su, H., Tanaja, J., Dec, E., Wallace, D.C., Mukherjee, J. *et al.* (2010) VCP associated inclusion body myopathy and Paget disease of bone knock-in mouse model exhibits tissue pathology typical of human disease. *PLoS One*, **5**, e13183.
56. Ross, J.M. (2011) Visualization of mitochondrial respiratory function using cytochrome c oxidase/succinate dehydrogenase (COX/SDH) double-labeling histochemistry. *J. Vis. Exp.*, **57**, e3266.
57. Jung, K.M., Clapper, J.R., Fu, J., D'Agostino, G., Guijarro, A., Thongkham, D., Avanesian, A., Astarita, G., DiPatrizio, N.V., Frontini, A. *et al.* (2012) 2-arachidonoylglycerol signaling in forebrain regulates systemic energy metabolism. *Cell Metab.*, **15**, 299–310.